Vol. XXII — No. 2 June, 1977

The SPEX Speaker

SPEX INDUSTRIES, INC. · 3880 PARK AVENUE · METUCHEN, N.J. 08840 · ☎ (201) -549-7144

APPLICATION OF RAMAN SPECTROSCOPY TO SNAKE TOXINS

Anthony T. Tu

Department of Biochemistry, Colorado State University, Fort Collins, CO 80523

From time immemorial snakes have been universally feared; and with good reason. Of the 2000-odd species slithering about every continent, except Antarctica, almost 300 are poisonous, their bite painful and dangerous if not always fatal. Even today, with antivenins kept in handy first-aid kits in much of the world, about 30,000 deaths are recorded each year from about one million snake bites. But the actual number of people killed probably exceeds this; most bites take place in tropical and sub-tropical rural regions where the cause of death more often than not remains unreported. Within seconds after being bitten by a monstrous king cobra in the forest, an Indian peasant falls over, dead. His body may not be found until long after evidence of the bite has been destroyed by scavenging insects.

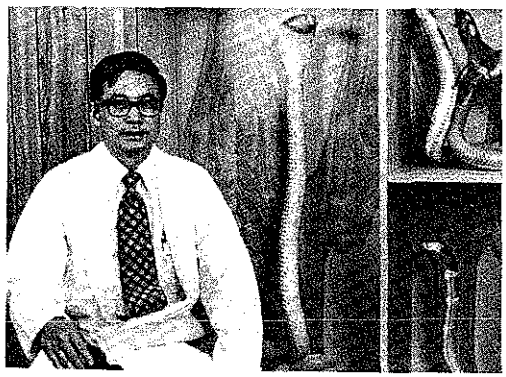

Of course, snakes aren't the only venomous members of the animal kingdom. People have learned to give wide berth to spiders, scorpions, fire ants, bees, wasps, hornets and lizards such as the Gila monster. Recently, the "killer" bee has attained well-deserved notoriety. Unlike most bees, it often attacks without provocation; its brutal bite can be fatal. Originally a hybrid in South America, the "killer" bee is relentlessly migrating northward at such a rate that it is expected in mainland U.S.A. in 10-20 years. Ironically, it is an unwanted hybrid, the result of an unfortunate human error in genetic engineering. The intent was to crossbreed gentle Brazilian bees of European origin with mean, but prolific, honey-producing African bees (*Apis mellifera adomsii*). Instead, the outcome boomeranged.

An understanding of the toxic factors in venoms is of great concern to pharmacologists and toxicologists. The venom from a "killer" bee, although quite similar chemically, can be differentiated from that of ordinary bees only by sophisticated analytical techniques. Apart from seeking such basic knowledge, scientists are hopeful of discovering compounds of possible therapeutic value. Finally, and of most current interest we hope to devise improved antivenins; a treatment applicable to all snake bite victims would be ideal.

Only limited success has been achieved thus far in formulating such combinations or polyvalent anti-venins. Although present ones do have the effect of simultaneously neutralizing the toxins of several snakes, their capacity for doing so is weak. And even more disappointing, the greater the number of anti-venins in a mixture, the poorer its neutralization efficiency against a specific venom. The only commercial formulation available in the U.S.A. originates from venoms of five different snakes native to North, Central, and South America. Although this anti-venin affords acceptable cross-reactive protection against these snakes, it is entirely ineffective for treatment of non-native snake bites. In our jet age, snakes as well as people have become international travelers. Inevitably, each year Americans are bitten by foreign snakes for which no anti-venins are locally available. The goal of developing a universal anti-venin is certainly desirable.

Analysis is necessarily the first step toward that goal. Snake venoms are exceedingly complex. Comprising about 90% protein, the kinds of protein as well as their proportions differ from species to species. In addition to proteins snake venoms contain an array of enzymes; in a collective sense, toxicity is due to both the enzymes and non-enzymatic proteins. Although the enzymes themselves are relatively non-toxic, they play a role in hemolysis, blood coagulation, blood anti-coagulation, autopharmacological and hemorrhagic effects. For the most part, however, the non-enzymatic proteins are the primary components responsible for toxicity.

Some venoms are predominantly neurotoxic and some are predominantly cardiotoxic. Neurotoxins disrupt nerve impulses and thereby paralyze muscles. Cardiotoxins, in a way not at all understood, stop the heart from beating. Depending on their species, American rattlesnakes fall into both categories. Additionally, their venom is necrotoxic—destructive of cellular tissue—and usually contains many other minor toxins.

Lethal Toxin of Rattlesnake Venom

Rattlesnakes are of particular interest to Americans since they are all-too-abundant in the United States, Central and South America. Unfortunately, to date, few toxins from rattlesnake venoms have been isolated and characterized. One is from the South American tropical rattlesnake (*Crotalus durisses terrificus*) and is very neurotoxic. Another is from the venom of Mojave rattlesnakes (*Crotalus scutulatus*) which is cardiotoxic. Yet another is a myotoxin—destructive of muscles—from the venom of Prarie rattlesnakes (*C. viridis viridis*). These venoms may, of course, contain other toxins which have not yet been isolated. Physiologic actions of rattlesnake venoms are complex. On envenomation, most rattlesnake bites induce severe necrosis; but because of the widespread availability of antivenins in the United States most people survive, although they may suffer loss of a finger or other extremity.

Mojave toxin, extensively studied by laser Raman Spectroscopy, has a molecular weight of 22,000 daltons and is an acidic protein (25), while most of the neurotoxins isolated from cobra and sea snake venoms are much smaller in size and are highly basic proteins. When the Raman spectra of Mojave toxin were examined, they showed

considerable differences from those sea snake neurotoxins (26). Raman spectra revealed that rattlesnake toxin contains predominantly α-helical structure and a tyrosine residue.

Neurotoxins

The venoms of sea snakes, cobras, kraits, and coral snakes all contain neurotoxins which strike the nervous system at specific points. Although in their action they resemble curare—the dart and arrow poison made by Indians from South American plants—neurotoxins employ entirely different mechanisms. Some toxins (puffer fish, DDT, scorpions) are neurotoxic because they inhibit nerve transmission at the axon, the impulse-transmitting part of a nerve cell (neuron). Others are neurotoxic because they inhibit nerve transmission at the neuromuscular junction (synapse) where a nerve fiber meets a muscle fiber. Neurotoxins found in snake venoms belong to the latter category. To complicate matters further, at the synapse, there are two sites; one is the nerve ending or "presynaptic site"; the other is the muscle face or "postsynaptic site." Some snake venoms (e.g., krait) contain neurotoxins that attack both sites while others (cobras and sea snakes) contain only the postsynaptic type of neurotoxins.

Chemistry of Neurotoxins

The chemical structure of many postsynaptic neurotoxins has been studied and, interestingly, they have all been found to be based on a very similar "peptide backbone," although the amino acid arrangement within the molecule may be different (see review articles (1) and (2)). Surprisingly, the postsynaptic neurotoxins contain two types of molecules. For convenience, the one with 8 sulfur atoms (4 disulfide bonds) is called Type I neurotoxin, and the one with 10 sulfur atoms (5 disulfide bonds) is called Type II neurotoxin (see Fig 2). Two-dimensional views of these two types of neurotoxins are shown in Fig 3.

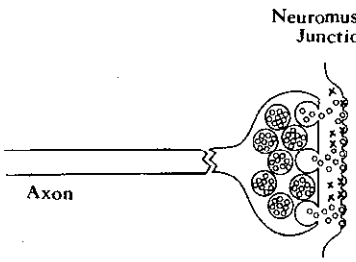

Fig 1 Highly schematic diagram showing the site of snake neurotoxins of the post-synaptic type. The snake neurotoxins (X) of this type actually attach to the acetylcholine receptor (—⌣—⌣—⌣—) in the muscle. Snake venom neurotoxins do not effect the "axon" portion of a nerve cell. When all the acetylcholine receptors are blocked by neurotoxins, the neurotransmitter, acetylcholine (o), cannot reach the post-synaptic site, thus the muscle is paralyzed. The left side of neuromuscular junction represents the "presynaptic site" while the right side is the "post-synaptic site (muscle)."

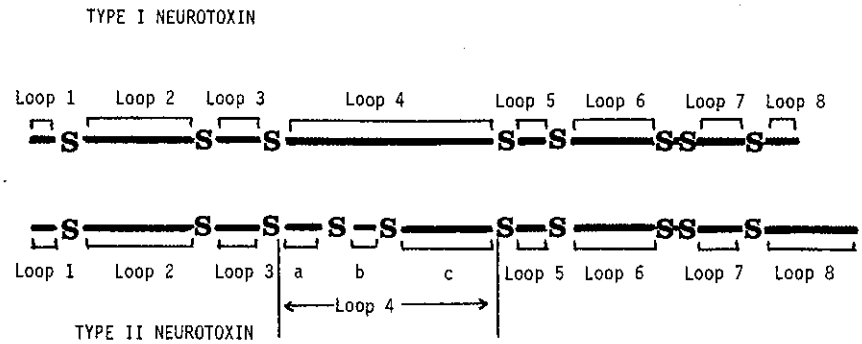

Fig 2 Schematic diagram of Type I and Type II neurotoxins showing similarities in the relative positions of half-cystine residue. Reprinted from *Ann. Rev. Biochem.*, 42, 246 (1973) by A.T. Tu.

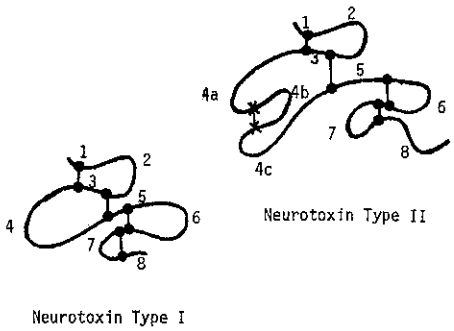

Fig 3 Two-dimensional structures of Type I and Type II neurotoxins. Note the antiparallel direction of the peptide backbones. The turns in the peptide backbone are β-turns. Both Type I and Type II are post-synaptic neurotoxins. It is of interest to note that cobra and krait venoms contain both types of toxins while sea snake venoms contain only Type I neurotoxins. The simplicity of neurotoxins in sea snakes reflects a more primitive nature for sea snakes than for terrestrial poisonous snakes.

Conformation of Proteins

As already mentioned, snake venoms are composed of a mixture of proteins, some toxic, others nontoxic. In order to study the chemical structure of a toxin, it must be isolated in pure form. Sometimes this is quite laborious. A common technique is, first, to remove the nontoxic proteins by taking advantage of their difference in molecular size through gel permeation chromatography . The toxins are further purified based on differences in charge using ion-exchange chromatography. When a pure toxin is attained, its three-dimensional structure is studied by several methods. All proteins consist of building blocks called amino acids joined together by peptide bonds. In studying the conformation (three-dimensional structure) of proteins, one must look at two aspects particularly. One is the peptide backbone structure or "secondary structure." The other is the arrangement of the many side chains in a protein or "tertiary structure." Of course, at times there is no clear dividing line between them. There are several typical types of peptide backbone arrangements such as "α-helix," "β-sheet structure," "β-turn conformation," "γ-turn conformation" and "random coil" (3). Some of these conformations are found to exist in snake toxins. For instance, all neurotoxins from cobra and sea snake venoms have β-sheet and β-turn conformations while a rattlesnake toxin contains α-helix.

Although no one physical method can elucidate all the structural aspects, X-ray diffraction is the most powerful. From it one can unequivocally deduce the absolute conformation of protein molecules. However, X-ray diffraction is only applicable to crystallized substances, and practically all protein molecules in the biological system are in aqueous solution. Thus, doubt always arises as to whether the conformational structure of proteins in the natural state is identical to the structure deduced by the X-ray diffraction method. Also, if crystallization cannot be achieved, X-ray diffraction fails altogether.

Fluorescence spectroscopy is another analytical tool for studying proteins. However, this method is inapplicable to the determination of peptide backbone structure and is rather limited in the study of the environment of the amino acid components, tyrosine and tryptophan. Complementing spectrofluorometry, circular dichroism (CD) is a powerful physical method for the study of protein structure, especially on the peptide backbone, but CD does not provide much structural information concerning side chains or disulfide bonds. To their disadvantage, both fluorescence and CD spectroscopies require aqueous solutions.

Raman spectroscopy overcomes most of these objections and recently has become popular for biological molecules such as proteins, nucleic acids, lipids, carbohydrates, heme compounds, and cell membranes. Raman spectroscopy can be carried out with crystal, powder, gel, or — unlike infrared — aqueous solution. Secondly, Raman can uncover information on the peptide backbone, geometry of disulfide bonds, and the environment of side chains such as tyrosine, tryptophan and methionine. Moreover, Raman can detect the presence of the disulfide bond (−S−S−), methionine residue, and sulfhydryl group (−SH) which is tedious by conventional chemical methods.

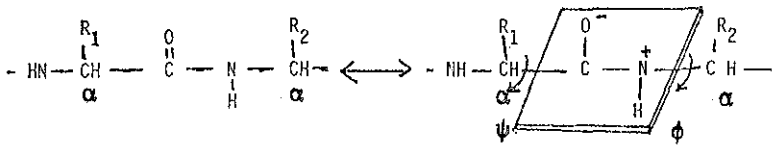

Scheme 1 The rotation of a peptide backbone is restricted to the C$_\alpha$—C (ψ) and N—C$_\alpha$ (ϕ) bonds. C$_\alpha$ represents the α carbon atom and is different from the carbon atom in the peptide bond, CONH. Spatial orientation of the peptide backbone (conformation) is determined by the angles of rotation of ψ and ϕ which are known as Ramanchandran angles. The peptide bond C(=O)—N(H) has no free rotation along the axis of C—N because C(=O)—N(H) lies in the same plane due to the resonance as shown in the above scheme.

Raman Spectra and Peptide Bonds

How can Raman spectroscopy elucidate protein structure? What is the theoretical basis for it?

As was mentioned before, all proteins consist of many peptide bonds.

The peptide bond is planar because of its resonance form as shown in Scheme 1. The bonds on both sides of a peptide bond, ψ and ϕ, (Ramanchandran angles) can be rotated. Depending on peptide backbone conformations, the angles ψ and ϕ are fixed and will ultimately affect the vibrational mode of a peptide bond.

A peptide bond gives rise to many different types of vibrational modes, such as Amide A and B bands, Amide I, II, III, IV, V, VI, VII bands (4). Among them, Amide I and III yield very prominent Raman bands spectra which are correlated with the structural property of protein molecules. Both Amide I and III bands arise from in-plane vibration of the peptide bond but are due to different modes of vibrations (Fig 4). From the Raman spectra of model compounds, it is known that α-helical structures generate an Amide I band at 1650 ± 5 cm^{-1} with strong intensity and sharp peak. The β-sheet structures also generate a strong and sharp Amide I line but at higher frequency of 1665 ± 5 cm^{-1}. Random coiled proteins usually yield a strong but broad Amide I band at about 1665 cm^{-1}. For the Amide III band, α-helical structures usually show a relatively weak band in the region of 1265 to 1300 cm^{-1}, while β-sheet structures show a strong line at 1235 ± 10 cm^{-1}. Random coil structure gives a medium intensity line at 1248 ± 10 cm^{-1} (5).

Raman Spectra and Disulfide Bonds

Disulfide bonds (−S−S−) help maintain the conformation of a protein and provide extra stability to a protein molecule; therefore, the understanding of disulfide bonds in a protein is quite important in the structural study of proteins. Raman spectroscopy is ideal for this purpose, furnishing information that other physical methods cannot. The origins of the S−S stretching vibrations have been extensively studied on model compounds. The S−S stretching vibration depends on the internal rotation about the C−S and C−C bonds, C−C−S−S−C−C (6). The Raman spectrometer can distinguish three types of disulfide bond geometry; namely, gauche-gauche-gauche, trans-gauche-gauche, and trans-gauche-trans conformation (Fig 5). From this kind of data one can readily piece together the structure of snake toxins.

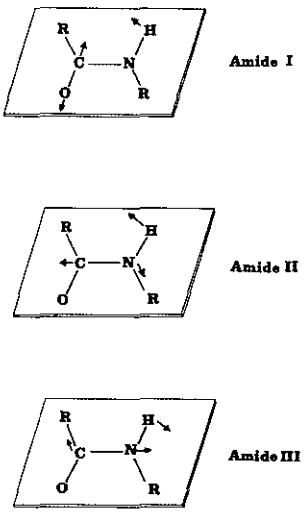

Fig 4 There are many different modes of the peptide bond vibration. The figure illustrates the "in-plane" vibrational modes of the peptide bond. Among the three modes shown in the figure, the Amide I and III are indices of peptide backbone conformation of a protein in the Raman spectra. The Amide II band is either Raman inactive or very weak.

Peptide Backbone Conformation of Snake Toxins

Unlike terrestrial snakes, sea snakes produce very small quantities of venom, ranging from 0.5 to 10 mg per snake depending on species and size. For our studies we captured 1000 sea snakes in the Indian Ocean and Pacific coasts in order to collect enough venom. Assembling enough venom turned out to be as difficult as actual research.

Several purified neurotoxins were extracted from different species of sea snake venoms. Without exception, prominent sharp Amide I bands at 1672 cm^{-1} appeared in the Raman spectra (Table 1). The Raman spectrum of

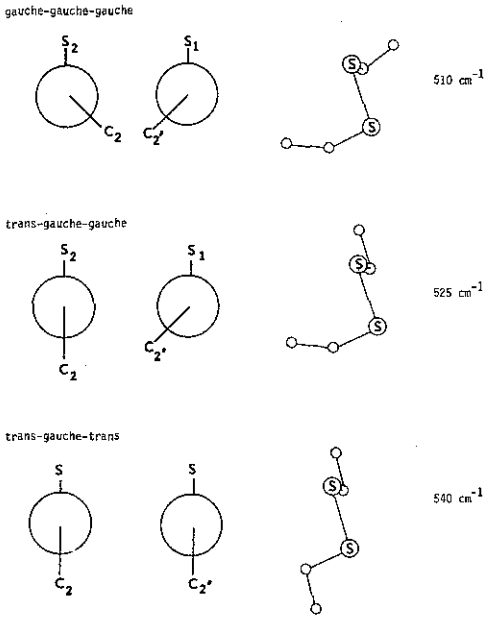

Fig 5 Conformation of disulfide bonds in proteins. The stretching vibration of S—S is influenced by the rotational conformation about the C—C and C—S bonds. The assignment numbers for C and S atoms are:

C_2-C_1-S_1-S_2-$C_{1'}$-$C_{2'}$

The disulfide bond with gauche-gauche-gauche shows a strong and sharp band in 510 cm^{-1}. The disulfide bonds with trans-gauche-gauche and trans-gauche-trans conformation give bands in 525 and 540 cm^{-1} in Raman spectra.

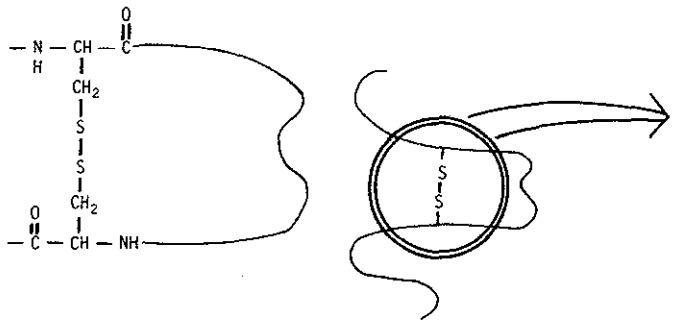

Scheme 2 The disulfide bond is very important in maintaining the conformation of proteins. The stretching vibration of this bond depends on the internal rotation of the C—S and C—C bonds of C—C—S—S—C—C. The diagram on the left shows in detail the structure of the disulfide bond. Normally it is expressed as —S—S— as shown in the diagram on the right.

Lapemis hardwickii (Hardwick's sea snake) neurotoxin is shown here as an example (Fig 6). The Amide III bands of purified neurotoxins ranged from 1240 to 1248 cm^{-1} (Table 1). From the high frequency of the Amide I bands and the low frequency of the Amide III bands, the possibility of an α-helix conformation for sea snake neurotoxins can be immediately excluded. But to differentiate β-structure from random coil structure by Raman spectra is more difficult. Fortunately, the chemical structures of many neurotoxins have been extensively studied and many structural properties are known. The amino acid sequence of many neurotoxins has been determined and the results show that they are very similar, especially with respect to position of disulfide bonds. Neurotoxins (Type I) are relatively small protein molecules with molecular weights of about 6800 daltons. The high stability of neurotoxins originates from the 4 disulfide bonds holding the peptide backbone tightly together, to provide a highly compact structure. From these chemical properties, it is almost impossible to conclude that neurotoxins contain a random coil because each loop is tightly held by disulfide bridges. Moreover, the conformation of two neurotoxins was studied by CD and was identified as a β-sheet structure (7, 8). Two-dimensional views of neurotoxins are also highly suggestive of being anti-parallel β-sheet structure (Fig 3). Consideration of all these facts and the results of Raman spectra led us to conclude that snake neurotoxins consist primarily of anti-parallel β-structures (9, 10).

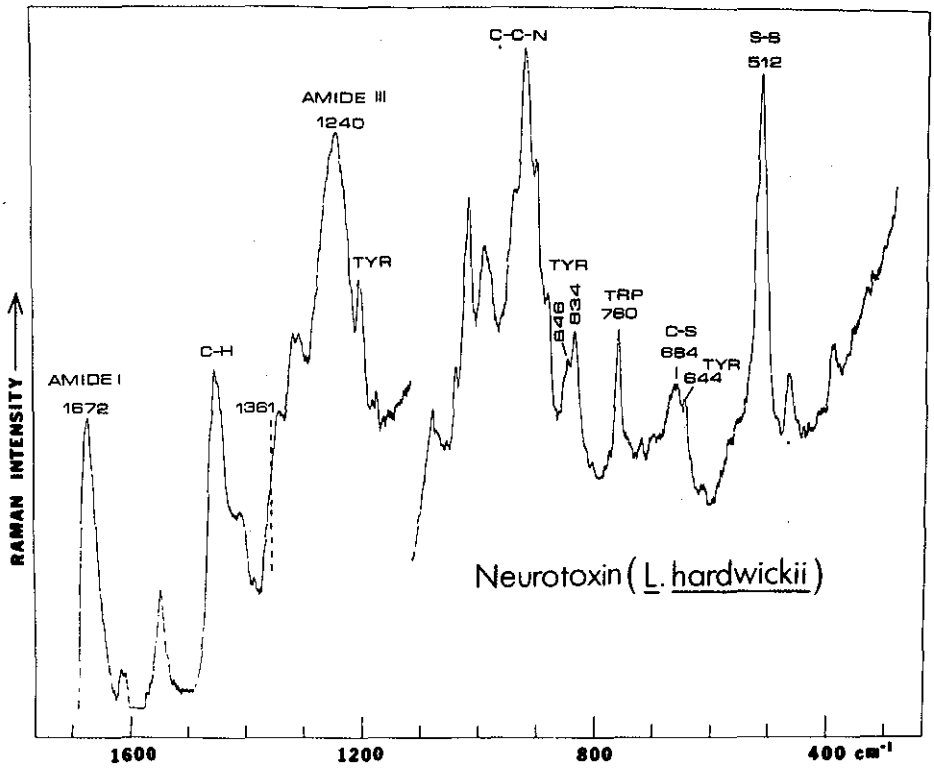

Fig 6 Raman spectrum of purified sea snake neurotoxin. Reproduced from *J. Biol. Chem.*, 250, 1782 (1975) by N.T. Yu, T.S. Lin, and A.T. Tu. Most sea snake toxins show similar Raman spectra as the *Lapemis hardwickii* neurotoxin. The major toxin of *Lapemis hardwickii* (Hardwick's sea snake) is used as an example in this figure. This indicates that most sea snake neurotoxins have very similar protein conformation regardless of the species and geographical origins of the sea snakes themselves. The spectrum is loaded with information on protein structure of the toxin. Amide I and III (1672 and 1240 cm^{-1}) bands indicate anti-parallel β structure of the toxin molecule. The lack of 1361 band indicates that the tryptophan group is exposed. The intensity ratio at 846 and 834 cm^{-1} indicates the tyrosine component is buried inside the fold of the toxin molecule. The disulfide stretching band is clearly shown at 512 cm^{-1} indicating the conformation of gauche-gauche-gauche.

Table 1. Characteristic Raman Lines of Snake Neurotoxins and Cobramine B.

Family	Hydrophiidae				Elapidae
Subfamily	Hydrophiinae			Laticaudinae	
Genus	Pelamis	Lapemis	Enhydrina	Laticauda	Naja
Species	platurus	hardwickii	schistosa	semifasciata	naja
Origin	Costa Rica	Thailand	Malaya	Philippines	India
Name / Bands	Pelamis Toxin a	Toxin	Toxin	Toxin b	Cobramine B
	(cm^{-1})	(cm^{-1})	(cm^{-1})	(cm^{-1})	(cm^{-1})
Amide I	1672	1672	1672	1672	1672
Heating	1664	-	-	-	-
Amide III	1245	1240	1242	1248	1235
Heating	1243 (broader)	-	-	-	-
-S-S	512	512	512	512	510
Heating	512 (major)	-	-	-	-
	546 (minor)	-	-	-	-
Reference	Tu et al., 1976	Yu et al., 1975	Yu et al., 1975	Tu et al., 1976	Yu et al., 1973

Shortly after the structure of sea snake neurotoxins was found to be anti-parallel β-structure by Raman spectroscopy (Fig 3), X-ray diffraction studies from two labs independently verified the conclusion (11, 12, 13). This is a milepost for Raman. Until then Raman spectroscopists had cautiously selected for study only those proteins previously characterized by X-ray spectroscopy.

As already stated, it is essential to ascertain whether the structure of a protein in solid phase is identical to that in the aqueous phase. Here Raman spectroscopy holds a tremendous advantage over other physical methods because it can be applied to both phases. Raman spectra of neurotoxins in solid and in aqueous solution showed identical Amide I and Amide III bands (9), confirming that the peptide backbone conformation of the neurotoxin is the same in the solid state and in solution. In view of the compact and stable molecule of neurotoxins, this is a reasonable finding. The anti-parallel β-sheet structure gives the appearance of a flat molecule with an "active surface." In addition to anti-parallel β-structure, snake neurotoxins also contain a "β-turn" structure (Fig 3), which was first predicted theoretically and later confirmed by X-ray diffraction (12, 14).

Disulfide Bridges in Snake Neurotoxins

There are four disulfide bridges in Type I neurotoxins and five in Type II neurotoxins (Fig 2). One of the most significant characteristics of snake neurotoxins is that they all contain a very high number of disulfide bridges (−S−S−). This is the prime reason why neurotoxins are so compact in molecular shape and possess such high stability.

Raman spectroscopy is especially powerful in determining the geometry of disulfide linkages. The fact that a very sharp and symmetrical peak at 512 cm^{-1} was obtained for all neurotoxins indicates that the four disulfide bonds present in the native toxins exhibit similar geometries (Fig 7). The observed 512 cm^{-1} S−S line originates from the gauche-gauche-gauche form. While Raman spectra of Type I neurotoxins were studied extensively, only one Type II neurotoxin was investigated (15); toxin B isolated from the Indian cobra (*Naja naja*). The S−S− stretching vibration of Toxin B showed a main peak at 510 cm^{-1} but also showed a shoulder at 523 cm^{-1}. This indicates that there is the trans-gauche-gauche conformation in addition to the main conformation of gauche-gauche-gauche form in Type II neurotoxins.

Side Chains of Snake Neurotoxins

Each sea snake neurotoxin molecule contains only one molecule of the amino acid, tyrosine, which is essential for toxic action (16). The tyrosine building block of a protein molecule is frequently responsible for its biological activity. However, its activity depends on whether it is buried inside the fold of a protein molecule or is exposed on the surface of the molecule. Sea snake neurotoxins contain a buried tyrosine (16). Dr. Nai-Teng Yu of Georgia Institute of Technology made a great contribution on this aspect of the tyrosine residue. He found that the relative intensities of the Raman lines at 830 cm^{-1} and 853 cm^{-1} are related to the environment of the tyrosine side chain (17). Working with the dipeptide, Gly-Tyr, as an example of exposed tyrosine, he found that the intensity ratio for the 853/828 cm^{-1} is 1.0:0.71 (Fig 8). An enzyme, RNase, is known to have "buried tyrosine residue" and the intensity ratio for 852/832 cm^{-1} is 1.0:0.8. On heating, the protein unfolds thus exposing the tyrosine residue, and this ratio is reversed (Fig 8).

From the Raman spectra of neurotoxins (Fig 6), it can be said that the single tyrosine residue is not readily accessible to the solvent and is perhaps involved in unusual binding with other side-chain residues. The laser-Raman analysis is in full agreement with the fact that only part of the tyrosine residue is nitrated when the Hardwick's sea snake and cobra neurotoxins are chemically modified (16, 18). This finding is also in full agreement with the result of fluorescent studies (8, 19).

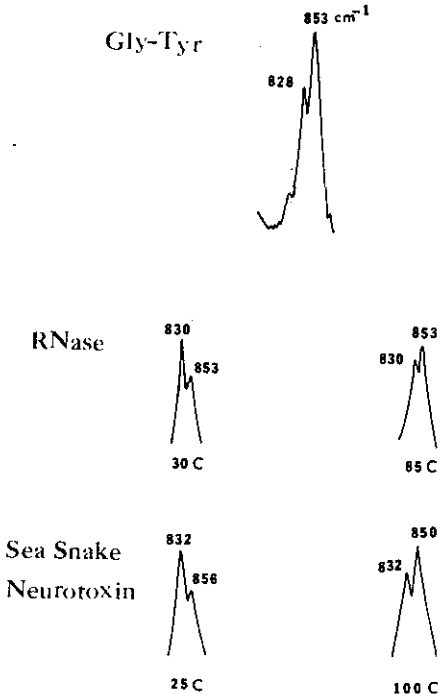

Fig 7 Raman spectrum of tyrosine residue. Gly-Tyr is used as a model of exposed tyrosine residues (Reproduced from *Arch. Biochem. Biophys.*, 156, 71 (1973) by N.T. Yu, B.H. Jo and D.C. O'Shea). The intensity ratio at 853/830 is reversed when RNase is heat denatured. This indicates that a tyrosine residue originally buried is now exposed by heat denaturization (Reproduced from *J. Am. Chem. Soc.*, 95, 5033 (1973) by N.T. Yu and B.H. Jo). The same phenomenon can be observed for sea snake neurotoxin (Reproduced from *Int. J. Peptide Prot. Res.*, 8, 337 (1976) by A.T. Tu, B.H. Jo and N.T. Yu).

Dr. Yu also found that the 1361 cm^{-1} band of another amino acid, tryptophan, in laser-Raman spectra is a very sensitive indicator of whether the tryptophan side chain is buried or exposed (20). When the tryptophan residue is buried and involved in certain interactions within a protein molecule, the 1361 cm^{-1} band shows a sharp peak. As the tryptophan residue becomes accessible to water molecules, the intensity of the 1361 cm^{-1} line diminshes. The lack of a distinct peak at 1361 cm^{-1} in the Raman spectra of neurotoxins (Fig 6) suggests that the single tryptophan residue is exposed. Again, results of Raman spectroscopy agree well with the results of studies involving chemical modification. That the single tryptophan residue of neurotoxins can be readily modified by different reagents indicates the tryptophan residue is exposed (21, 22). Both tyrosine and tryptophan residue are considered essential for the biological activity of Type I neurotoxins (23).

Raman spectroscopy can also detect methionine residue; its C−S stretching vibration appears at 700 cm^{-1}. Pelamis toxin *a*, isolated from the venom of *Pelamis platurus* (yellow-bellied sea snake), contains one mole of methionine (23) while toxin *b* obtained from the venom of *Laticauda semifasciata* (broad-banded blue sea snake) is free of any methionine residue (24). In their respective spectra, the former yields a line at 701 cm^{-1} and the latter does not (10). This illustrates Raman spectroscopy's potential not only for conformational study, but also for a quick and simple analytical assay.

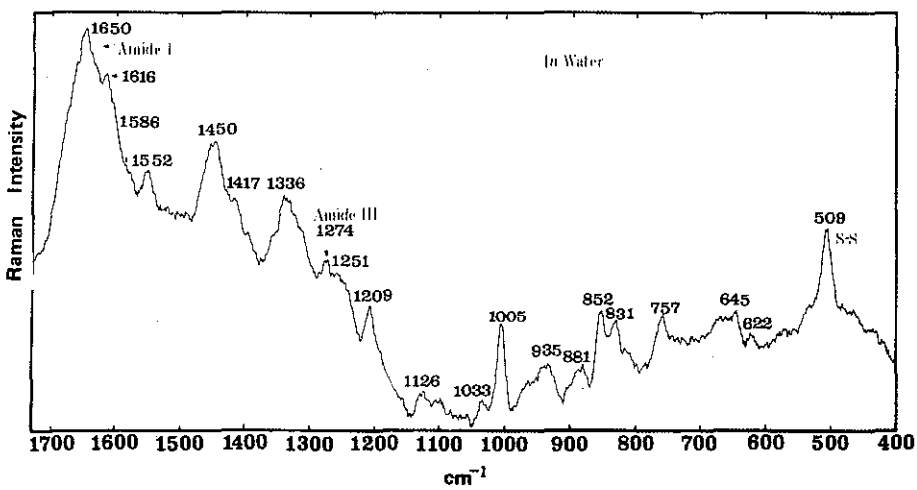

Fig 8 Raman spectrum of Mojave toxin isolated from Mojave rattlesnake venom (Reproduced from *Biochem. Biophys. Res. Comm.*, 68, 1139 (1976) by A.T. Tu, B. Prescott, C.H. Chou, and G.J. Thomas). The Amide I and Amide III region by the 1650 and 1274 cm^{-1} frequencies, respectively, is a clear indication of a predominantly α-helical backbone conformation. In contrast to Mojave toxin, sea snake neurotoxins predominantly consist of anti parallel β and β-turn structures (Fig. 3, Fig. 6). The appearance of a strong and sharp line at 509 cm^{-1} is due to four disulfide linkages. The sharp and symmetrical shape of this line indicates a high probability that the geometrics of all four disulfide linkages are similar. The intensity ratio of 0.71 for 828:853 cm^{-1} is indicative of exposed (completely solvated) tyrosol groups. Probably the tyrosine components are located on the surface of the protein molecule.

Conclusion

Although it is uniquely applicable in many respects, Raman spectroscopy is hardly sufficient; no single discipline can be expected to probe the secrets of complex protein molecules. To fully examine the structural properties of a toxin, every possible physico-chemical process must be applied. As data is accumulated from the many complementary analytical techniques, the vast complexity of venoms untangles and progress in formulating antivenins advances.

REFERENCES

1. Tu, A.T. (1973) Neurotoxins from animal venoms: Snakes, *Ann. Rev. Biochem.*, **42**, 235.
2. Tu, A.T. (1977) *Venoms: Chemistry and Molecular Biology*, John Wiley, New York, 560 pages.
3. Deber, C.M.; Madison, V.; and Blout, E. R. (1976) Why cyclic peptides? Complementary approaches to conformations, *Accounts of Chem. Res.*, **9**, 106.
4. Miyazawa, T. (1967) "Infrared spectra and helical conformations," in G. D. Fasman, Ed., *Poly-α-Amino Acids*, Marcel Dekker, New York, p. 69.
5. Thomas, G. J., and Murphy, P. (1975) Structure of coat proteins in Pf1 and fd virions by laser Raman spectroscopy, *Science*, **188**, 1205.
6. Sugeta, H.; Go, A.; and Miyazawa, T. (1973) Vibrational spectra and molecular conformation of dialkyl disulfides, *Bull. Chem. Soc.*, **46**, 3407.
7. Yang, C.C.; Chang, C.C.; Hayashi, K.; Suzuki, T.; Ikeda, K.; and Hamaguchi, K. (1968) Optical rotatory dispersion and circular dichroism of cobrotoxin, *Biochim. Biophys. Acta*, **168**, 373.
8. Hauert, J.; Maire, M.; Sussman, A.; and Bargetzi, J. P. (1974) The major lethal neurotoxin of the venom of *Naja naja philippinensis*: Purification, physical and chemical properties, partial amino acid sequence, *Int. J. Peptide Protein Res.*, **6**, 201.
9. Yu, N. T.; Lin, T. S.; and Tu, A. T. (1975) Laser Raman scattering of neurotoxins isolated from the venoms of sea snake *Lapemis hardwickii* and *Enhydrina schistosa*, *J. Biol. Chem.*, **250**, 1782.
10. Tu, A. T.; Jo, B. H.; and Yu, N. T. (1976) Laser Raman spectroscopy of snake venom neurotoxins: Conformation, *Int. J. Peptide Prot. Res.*, **8**, 337.
11. Tsernoglou, D., and Petsko, G. A. (1976) The crystal structure of a post-synaptic neurotoxin from sea snake , *FEBS Letters*, **68**, 1.
12. Low, B. W.; Preston, H. S.; Sato, A.; Rosen, L. S.; Searl, J. E.; Rudko, D. D.; and Richardson, J. S. (1976) Three-dimensional structure of erabutoxin b neurotoxic protein, Inhibitor of acetylcholine receptor, **73**, 2991.
13. Tsernoglau, D.; Petsko, G. A.; and Tu, A. T. (1977) Protein sequencing by computer graphics, *Biochem. Biophys. Acta*, **491** 605.
14. Chen, Y. H.; Lu, H. S.; and Lo, T. B. (1975) Conformation of snake neurotoxins: Prediction and comparison, *J. Chin. Biochem. Soc.*, **4**, 69.
15. Takamatsu, T.; Harada, I.; Shimanouchi, T.; Ohta, M.; and Hayashi, K. (1976) Raman spectrum of toxin B in relation to structure and toxicity, *FEBS Letters*, **72**, 211.
16. Raymond, M. L., and Tu, A. T. (1972) Role of tyrosine in sea snake neurotoxin, *Biochim. Biophys. Acta*, **285**, 498.
17. Yu, N. T.; Jo, B. H.; and O'Shea, D. C. (1973) Laser Raman scattering of cobramine B, a basic protein from cobra venom, *Arch. Biochem. Biophys.*, **156**, 71.
18. Menez, A.; Morgat, J.; Fromageot, P., Ronseray, A.; Boquet, P.; and Changeux, J. P. (1971) Tritium labeling of the α-neurotoxin of Naja nigricollis, *FEBS Letters*, **17**, 333.
19. Bukolova-Orlova, T. G.; Burstein, E. A.; and Yukel'son, L. Ya (1974) Fluorescence of neurotoxins from middle-Asian cobra venom, *Biochim. Biophys. Acta*, **342**, 275.
20. Yu, N. T. (1974) Comparison of protein structure in crystals, in lyophilized state, and in solution by laser Raman scattering, III. α-Lactalbumin, *J. Am. Chem. Soc.*, **96**, 4664.
21. Hong, B. S., and Tu, A. T. (1970) Importance of tryptophan residue for toxicity in sea snake venom toxins, *Fed. Proc.*, **29**, 888.
22. Tu, A. T., and Hong, B. S. (1971) Purification and chemical studies of a toxin from the venom of *Lapemis hardwickii* (Hardwick's sea snake), *J. Biol. Chem.*, **246**, 2772.
23. Tu, A. T.; Lin, T. S.; and Bieber, A. L. (1975) Purification and chemical characterization of the major neurotoxin from the venom of *Pelamis platurus*, *Biochemistry*, **14**, 3408.
24. Tu, A. T.; Hong, B. S.; and Solie, T. N. (1971) Characterization and chemical modifications of toxins isolated from the venoms of sea snake, *Laticauda semifasciata* from the Philippines, *Biochemistry*, **10**, 1295.
25. Bieber, A. L.; Tu, T.; and Tu, A. T. (1975) Studies of an acidic cardiotoxin from the venom of Mojave rattlesnake (*Crotalus scutulatus*), *Biochim. Biophys.* Acta, **400**, 178.
26. Tu, A. T.; Prescott, B.; Chou, C. H. and Thomas, G. J. (1976) Structural properties of Mojave toxin of *Crotalus scutulatus* (Mojave rattlesnake) determined by laser Raman spectroscopy, *Biochem. Biophys. Res. Comm.*, **68**, 1139.

RECENT REWARDING RAMAN RESULTS

Our new 1478 SPATIAL FILTER; an argon ion pumped rhodamine 6G dye laser; computer massaging; and a couple of new Ramalog accessories have netted a spate of spectra well worth sharing.

1. POLYPEPTIDES

Real-world samples encountered in pharmaceutical research tend toward the nightmarish to a Raman spectroscopist. Principally because they harbor impurities, they fluoresce. And because fluorescence intensities tend to sprawl many orders of magnitude over Raman intensities, Raman spectra remain hidden in the background noise. Exciting with a dye laser wavelength longer than that which stimulates fluorescence offers an opportunity to separate out the shifted Raman spectrum. Coupled with signal averaging and finally with smoothing computer functions, S emerges victorious over N.

Several stubborn samples recently responded beautifully to this treatment. One was a polypeptide the secondary structure of which was being studied. Its Raman spectrum seemed unattainable when attempted with the 514.5 nm argon ion laser line because of the high fluorescence level and rapid sample decomposition. Although both were virtually eliminated with dye laser excitation at 595.2 nm, the resulting Raman spectrum, a single scan, was weak and indefinite (1A). Repetitive scanning, background subtraction, and curve smoothing through the SC4 SpexComp Spectrometric Computer System produced the extensive and relevant spectral features revealed in Spectrum 1B.

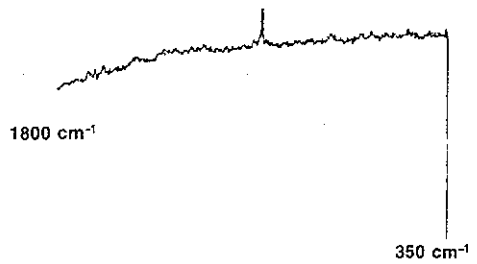

Spectrum 1A: Single-scan, directly-recorded Raman spectrum of a polypeptide with 595.2 nm rhodamine 6G dye laser excitation.

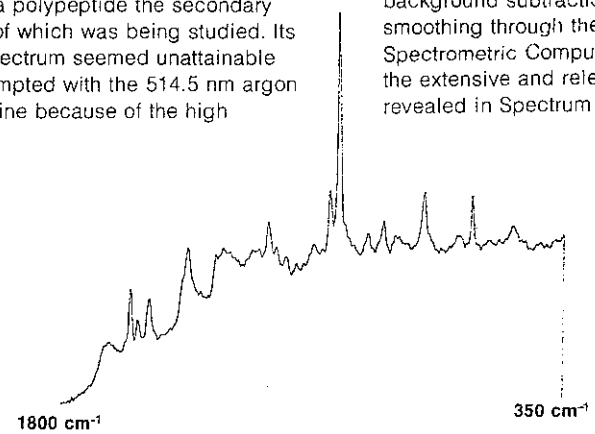

Spectrum 1B: Background-subtracted, 20-scan signal averaged, smoothed Raman spectrum of the polypeptide sample.

2. RETAINED MONOMERS IN POLYMETHYL METHACRYLATE (PMM)

The FDA has been looking askance at monomers retained in PMM implantable lenses. These tiny, precision-molded bits of plastic are the closest conceivable second best to nature's own and a very welcome exchange for those that are cataract-beclouded. But reactive monomers or catalysts must be monitored, and Raman proves remarkably efficient for the task. A well-defined monomer band is seen at 1640 wavenumbers in Spectrum 2. The ratio of intensity of this band to that at 1730 wavenumbers is related quantitatively to the concentration of retained monomer—put another way, the degree of polymerization. Fast and non-destructive, the method is well suited to routine quality control inspection.

We are indebted to Dr. R. Kenneth Epling of Coburn Optical Industries for providing samples of the implantable lenses and alerting us to the procedure developed by Dr. Ian K. Pasco while at Brunel University, England.

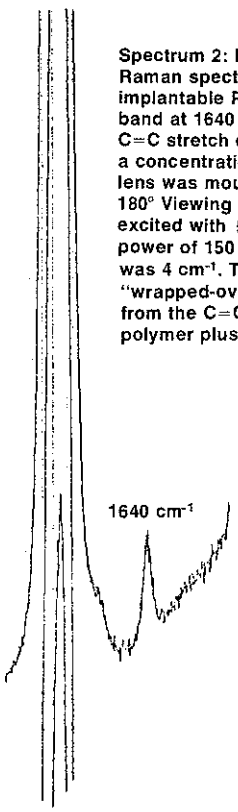

Spectrum 2: Portion of a Raman spectrum of an implantable PMM lens. The band at 1640 cm⁻¹ arises from C=C stretch of the monomer at a concentration of 0.6%. The lens was mounted on the Spex 180° Viewing Platform and was excited with 514.5 nm laser power of 150 mW. Bandpass was 4 cm⁻¹. The adjoining, strong "wrapped-over" line arises from the C=O stretch of the polymer plus monomer.

1478 SPATIAL FILTER

With this accessory we have achieved a dramatic enhancement of the low-frequency Raman performance of our 1400-series double spectrometers. Directing light from the first half of the spectrometer through two instead of one intermediate slit, the multi-component Spatial Filter rejects the troublesome laser excitation frequency while freely passing the shifted Raman radiation, keeping maximum throughput. See Spectra 3 and 4 below.

3. POLYETHYLENE OXIDE (PEO) — (WITH 1478 SPATIAL FILTER)

PEO drawn through a die, has shown strengths approaching that of metals in short lengths of equal cross-section. As yet a laboratory curiosity, the Herculean polymeric strands show 10-15 wavenumber Raman structure that appears to be a salient clue, possibly originating from an accordian-like vibration. The intensity of the band is affected by various tempering and annealing processes and is clearly revealed in Spectrum 3 by the Ramalog 5M which incorporates the new 1478 Spatial Filter accessory.

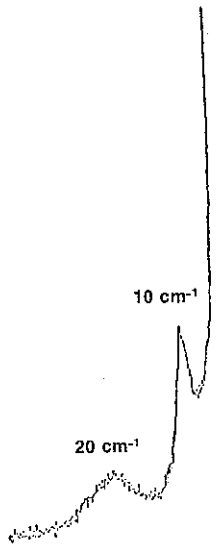

Spectrum 3: Low-frequency spectrum of polyethylene oxide taken with 1478 Spatial Filter on RAMALOG 5M. The powder was inside a glass capillary. Laser power, 100 mW at 514.5 nm; Bandpass, 0.5 cm⁻¹; Scan speed, 0.02 cm⁻¹/sec.; photon counting scale 2000 fs; Claassen filter.

4. MOLYBDENUM DISULFIDE — (WITH 1478 SPATIAL FILTER)

Similar structurally to graphite, MoS_2 crystals are also noted for their lubricating property. Although they consist of flat layers sandwiched together by smooth "slip" planes, they are hardly smooth to Raman spectroscopists, who must contend with finding a 30-wavenumber band for a substance that is black and shiny. The Ramalog 5M prevailed, producing the noteworthy Spectrum 4.

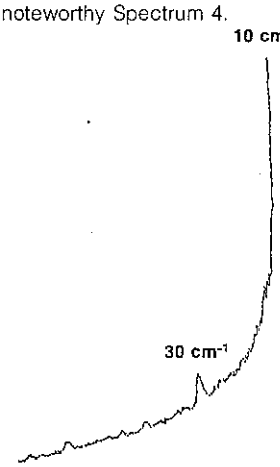

Spectrum 4: Low-frequency spectrum of a pressed pellet of MoS_2 taken with 1478 Spatial Filter on RAMALOG 5M. Laser power, 100 mW at 514.5 nm; Bandpass, 1 cm⁻¹/sec.; photon counting scale 10k fs; Claassen filter.

1456 FINE ALIGNMENT PLATFORM

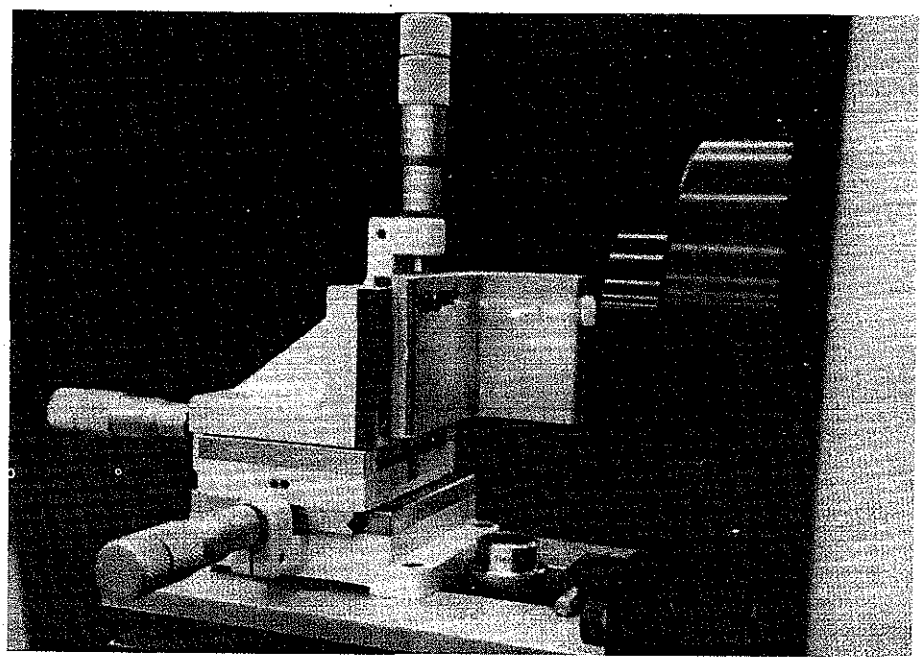

Close to being a universal mount for Raman spectroscopy, this new accessory is a precision, 3-axis manipulator mounted kinematically in the illuminator of the RAMALOG. Four tapped holes allow for fashioning one's own holders for odd-shaped samples. A small, 3-finger chemical clamp can be swiveled on a horizontal axis as a further aid in rapid alignment. It takes just a bit of ingenuity to wax a small sample on the face of the manipulator or even hold the sample with a rubber band. Once held, the sample may be adjusted along three orthogonal axes by means of individually controlled micrometer heads reading to 0.001" with a total travel of 0.5".

Two unusual analytical accomplishments illustrate the versatility of the 1456 accessory:

I. BUBBLES IN GLASS.

In the manufacture of high-quality glass, the presence of internal bubbles is not only undesirable cosmetically, but adversely affects optical properties as well. In lenses internal bubbles degrade image quality, while in mirrors surface bubbles result in scattering pock-marks during grinding.

Since all information regarding the origin of bubbles in glass is important in tracing their origin, an analysis of the gases inside is highly desirable. Well suited is Raman Spectroscopy. It is non-destructive, able to examine small cross sections of material, and is highly specific.

Blocks of glass about 1 cm on a side containing internal bubbles ranging from 0.1 to 0.5 mm in diameter were examined. Polished on all six sides, the blocks were mounted on a 1456 Fine Alignment Platform in order to allow accurate alignment in all three axes. Because the glass fluoresced slightly, the path of the laser traversing the glass could be observed and aligning and focusing the laser beam inside the bubble were easily accomplished.

An Ar laser provided 1.6 watts of power at 5145A. Set to a bandpass of 5 cm^{-1} and a scanning speed of 0.2 cm^{-1}/sec, the RAMALOG generated weak lines of oxygen and carbon dioxide from bubbles in one sample. In another, bands of nitrogen and oxygen appeared in a ratio equal to that of air. It should be pointed out that the scattering level hovered around 20-50 cps, requiring a photomultiplier with an exceptionally low dark count (around 3 cps, cooled).

II. HEADSPACE ANALYSIS IN GLASS AMPOULES

In the pharmaceutical industry, many of the drugs supplied in sealed glass ampoules are easily oxidizable. It is, therefore, common practice to add reducing agents as preservatives and to flush the ampoules with an inert gas to displace air prior to sealing. Because of its selectivity and nondestructive nature, Raman spectroscopy is ideally suited as a monitor of both the liquid (for decomposition products) and the headspace (for residual oxygen content) in a quality control application.

Experimental conditions were similar to that in Part I with the ampoules aligned at an angle to allow the laser beam to pass through the headspace without coming in contact with the solution.

Several ampoules with varying N_2/O_2 ratios were checked for the intensity of the N_2 band at 2331 cm^{-1} and that of the O_2 band at 1558 cm^{-1}. In air the ratio of N_2/O_2 band intensity was found to be 2.9/1 while in the headspace of a water-filled ampoule sealed in air the ratio was found to be 3.3/1. The slight increase in N_2/O_2 ratio can be explained by the higher solubility of O_2 in water than N_2.

As the presence of O_2 in the ampoule decreased, the N_2/O_2 band intensity increased until, at the minimum detectable level of 0.6% O_2 in N_2, a ratio of 65/1 was obtained. With a more powerful laser, lower levels of O_2 could undoubtedly be detected.

SPEX INDUSTRIES, INC./ P.O. BOX 798/METUCHEN, N. J. 08840/ ☎ (201) 549-7144